Beta-delayed two-proton decays of ^{22}Al and ^{26}P

M. D. Cable, J. Honkanen,* E. C. Schloemer, M. Ahmed, J. E. Reiff, Z. Y. Zhou,† and Joseph Cerny
Department of Chemistry and Lawrence Berkeley Laboratory, University of California, Berkeley, California 94720
(Received 22 June 1984)

Beta-delayed two-proton radioactivity has been observed for the two nuclei ^{22}Al and ^{26}P. Proton-proton coincidence experiments performed at small and large angles show that the dominant two-proton emission mechanism is a sequential process. Decay schemes have been determined for each isotope.

I. INTRODUCTION

Beta-delayed two-proton radioactivity is a new decay process originally predicted by Gol'danskii in 1980.[1] This process involves the relatively slow beta decay of an isotope to an excited state of its daughter, which subsequently decays by the rapid emission of two protons. In particular, Gol'danskii predicted that should the then unknown isotopes ^{22}Al and ^{26}P exist, they would be prime candidates to exhibit this decay mode. Recent studies of the beta-delayed proton decay of these two isotopes[2,3] showed not only that they do exist, but provided a measurement of the masses of the lowest $T=2$ analog states in the beta decay daughters which are fed by superallowed beta decay. These states were thus shown to be unbound to the emission of two protons, as predicted, and subsequent proton-proton coincidence experiments[4,5] detected the first known cases of beta-delayed two-proton radioactivity.

Both ^{22}Al and ^{26}P exhibit this decay mode. Figures 1 and 2 show the similar decay schemes for each of these odd-odd, $T_z=-2$ isotopes. Using the ^{22}Al decay as an example, ^{22}Al will be referred to as the precursor, ^{22}Mg as the emitter, and ^{21}Na and ^{20}Ne as the proton and two-proton daughters, respectively. Because of the relatively large superallowed beta branch to the $T=2$ analog state in the emitter nucleus, decay modes involving this state are most readily observed experimentally, and unless explicitly stated otherwise, all decay branches discussed in this work will involve the analog state.

It can be seen from Figs. 1 and 2 that a variety of decays of the analog states are energetically possible. Particle emissions in the forms of α, p, or 2p decay all have several MeV of decay energy and are all expected to contribute to the total decay. Alpha particles of the energies expected are not observable in the experimental work to be described, and will not be discussed. One notable difference between the ^{22}Al and ^{26}P decays is that ^{2}He emission (a two-proton emission mechanism discussed further in the following) is spin-parity forbidden for the ^{26}P beta-delayed two-proton branch ending in the ^{24}Mg ground state. This makes a comparison of these decays especially useful for a characterization of two-proton emission mechanisms. Beta-delayed proton decay of both ^{22}Al and ^{26}P has been discussed in Refs. 2 and 3, and results of the measurements, such as the masses of the analog states, will be used here without describing the experimental work in detail. The focus of this paper will be to summarize all the experimental work on the beta-delayed two-proton decay branch and to relate this to possible decay mechanisms for two-proton emission.

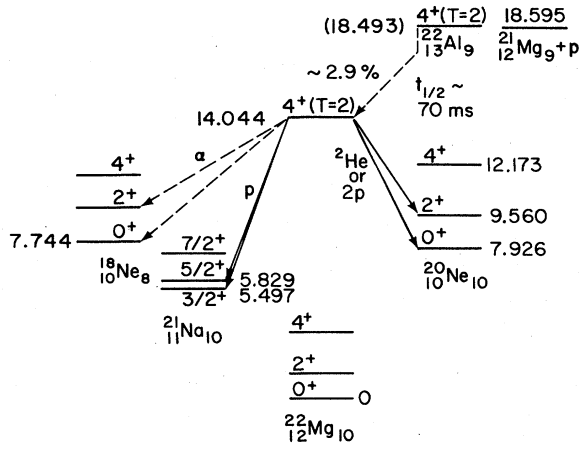

FIG. 1. Proposed partial decay scheme for ^{22}Al.

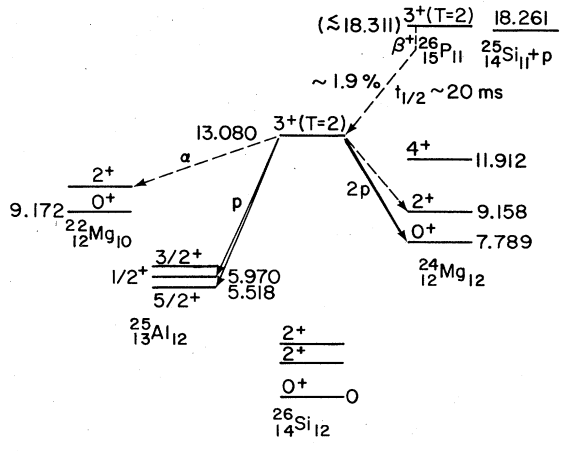

FIG. 2. Proposed partial decay scheme for ^{26}P.

II. TWO-PROTON EMISSION MECHANISMS

Since two-proton emission from a relatively long-lived state such as these $T=2$ analog states (particle emission is slowed because it is isospin forbidden) has never been observed, the question of how these protons will leave the nucleus is an interesting one. Much of the early theoretical work of Gol'danskii on direct two-proton radioactivities[6] is applicable here. Drawing on this as background, several possible decay mechanisms will be presented.

One possibility is that the protons will leave the nucleus coupled to a $^1S_0$ configuration. This process will be referred to as ^{2}He emission. The virtual state, ^{2}He, has been studied in reaction work (for example, Ref. 7 or 8), and for our purposes, can be thought of as a proton pair penetrating the Coulomb and angular momentum barriers of the nucleus with a virtual energy, ϵ, shared between the protons. This center-of-mass energy of the proton pair then "returns" at some distance from the nucleus as kinetic energy of the protons which are now correlated at small angles. For simplicity, this discussion (in particular, the Monte Carlo simulations described in the following) will assume this breakup occurs well outside the Coulomb and angular momentum barriers. This simplification has very little effect on the observable experimental properties.

For ^{2}He emission, momentum and energy conservation give the following expression for the summed laboratory energy of the two protons:

$$E^L=\frac{mE_{\text{c.m.}}+2m_p\epsilon+\epsilon^2}{m+2m_p+\epsilon}\ , \tag{1}$$

where $E_{\text{c.m.}}$ is the center-of-mass decay energy for the two protons, ϵ is the relative energy of the two protons (sometimes called the breakup energy), m_p is the mass of the proton, and m is the mass of the two-proton daughter (for ^{22}Al, the mass of ^{20}Ne). The quantity ϵ is determined by the nucleon-nucleon interaction of the proton pair (commonly referred to as the final state interaction) and is expected from reaction work (again, for example, Ref. 7 or 8) to appear as a distribution with a maximum value of $\sim$500 keV and a FWHM of $\sim$600 keV.

Given a value for ϵ, the kinematic expressions for laboratory energies and angles of the protons are a standard problem solved in many texts such as Ref. 9 or 10. For the purposes of this discussion, it is sufficient to summarize this calculation with the expression

$$\cos\eta=\frac{E_1^L+E_2^L-2\epsilon}{2(E_1^LE_2^L)^{1/2}}\ , \tag{2}$$

where η is the relative laboratory angle between the protons, and E_1^L,E_2^L are individual proton laboratory energies ($E_1^L+E_2^L=E^L$). η is maximized for $E_1^L=E_2^L$, and this is also expected to be its most probable value; therefore, the individual proton spectrum from ^{2}He emission should be a distribution, symmetric about $E_1^L=E_2^L$ with its shape determined by the final state interaction (the distribution in ϵ) and also by the detector efficiency variation as a function of η. The expected appearance of the ^{2}He spectra in the laboratory is calculated through Monte Carlo simulations presented in the following, after the detector systems have been described.

Another class of decay mechanisms besides ^{2}He emission will be categorically referred to as uncoupled mechanisms. An uncoupled mechanism can be thought of as two protons independently leaving the nucleus with a time, Δt, between the first and second emission. If Δt is long enough for the formation of an intermediate state of the proton daughter nucleus, then this process will be referred to as a sequential emission. The alternative case ($\Delta t \lesssim 10^{-21}$ s) will be referred to as preequilibrium emission.

Sequential emission is in many ways similar to a gamma ray cascade. Two protons, each with a discrete decay energy dependent upon the intermediate state energy, will be emitted. For sequential emissions where neither proton has $l=0$ and the intermediate state spin is not $\frac{1}{2}$, angular correlations are expected. For protons, however, these angular correlations are not expected to be large (a $<$10—20% effect from calculations based on methods described in Ref. 11) and for most of this work will not be discussed, since the experiments described in the following could not distinguish between weakly correlated distributions and isotropic emission. As in gamma ray cascades, the second proton is emitted from a recoiling nucleus and the conversion from center-of-mass to laboratory energies must account for this fact. Unlike gamma rays, however, protons are relatively massive and this recoil effect is quite large; it will, in fact, be a major factor in identification of a two-proton decay as a sequential emission.

For sequential emission, expressions for the laboratory energies of the two individual protons are

$$\begin{aligned} E_1^L&=\left[\frac{m_1}{m_2}\right]E_1\ , \\ E_2^L&=\left[\frac{m}{m_1}\right](E_{\text{c.m.}}-E_1)+\frac{E_1(m_p)^2}{(m_1)(m_2)} \\ &\quad -\frac{2m_p\cos\theta}{m_1}\left[\frac{mE_1(E_{\text{c.m.}}-E_1)}{m_2}\right]^{1/2}\ , \end{aligned} \tag{3}$$

where symbols not in Eqs. (1) or (2) are defined as follows:

m_1 is the mass of the intermediate state in the proton daughter (for ^{22}Al, the mass of ^{21}Na*), m_2 is the mass of the two-proton emitter state (for ^{22}Al, the mass of ^{22}Mg*), E_1 is the center of mass decay energy for proton one, and θ is the center of mass angle between the protons.

It can be seen that the first proton in sequential emission has the usual laboratory energy calculated as in single proton emission but that the second proton laboratory energy is a function of θ. Again, Monte Carlo simulations of expected observable proton spectra will be presented in the following.

A detailed description of preequilibrium emission (Δt short) of two protons would involve a knowledge of the evolution of the nucleus following the emission of the first proton. This makes such a treatment quite difficult, and we shall only discuss the qualitative features of the relatively simple, limiting case of $\Delta t=0$. For this case, if possible spin-dependent angular correlations are negligibly small as in sequential emission, and ignoring barrier penetrabilities, then phase space limitations will determine

the proton energy spectrum; the appropriate kinematics are readily soluble. Individual proton spectra for the $\Delta t=0$ case will again, as in ^{2}He emission, consist of a continuum of proton energies with equal p_1 and p_2 energies being the most probable case. Unlike ^{2}He emission, however, these protons are not restricted to small angles and there is an angular dependence for their laboratory energies similar to that of sequential emission. Monte Carlo simulations for the $\Delta t=0$ case of preequilibrium emission will be discussed in the following.

III. EXPERIMENTAL METHOD AND MONTE CARLO SIMULATIONS

^{22}Al ($t_{1/2}\sim 70$ ms) and ^{26}P ($t_{1/2}\sim 20$ ms) were produced via the ^{24}Mg(^{3}He,p4n)^{22}Al and ^{28}Si(^{3}He,p4n)^{26}P reactions with 110 MeV ^{3}He^{+2} beams of 3–7 μA intensities from the Lawrence Berkeley Laboratory's 88-Inch Cyclotron. Recoiling product nuclei were stopped in $\sim$1.3 atm helium and transported to a detector chamber with the helium jet apparatus shown schematically in Fig. 3. NaCl was used as an additive to improve speed and transport efficiency through the 70 cm (1.3 mm i.d.) capillary. Transported activity was collected on a catcher wheel to form a source for particle spectroscopy with the solid state telescopes described in the following. Long-lived beta activities were reduced by a slow rotation of the catcher wheel with further removal of beta background accomplished by magnets and collimators. All data were recorded event by event on a ModComp Classic computer using the data acquisition and analysis program CHAOS,[12] enabling the use of several software particle identification techniques.

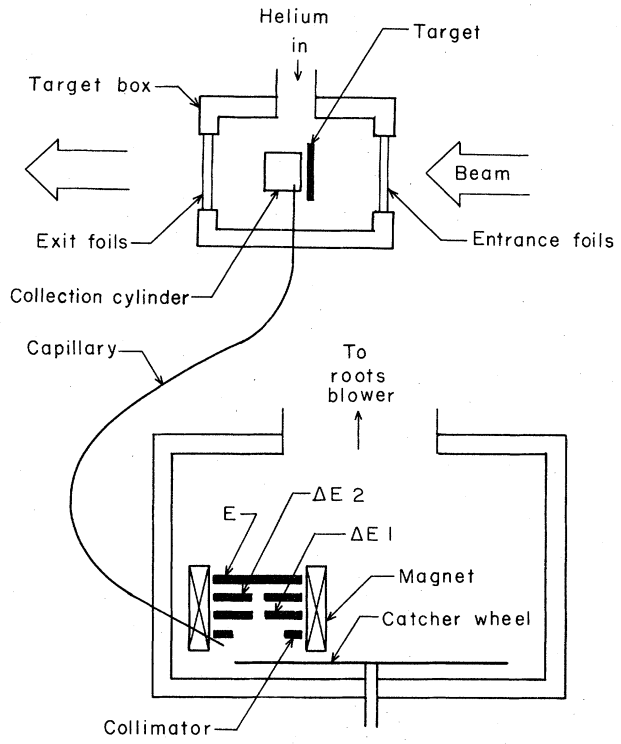

FIG. 3. Schematic diagram of helium jet apparatus. Small angle detector system is shown.

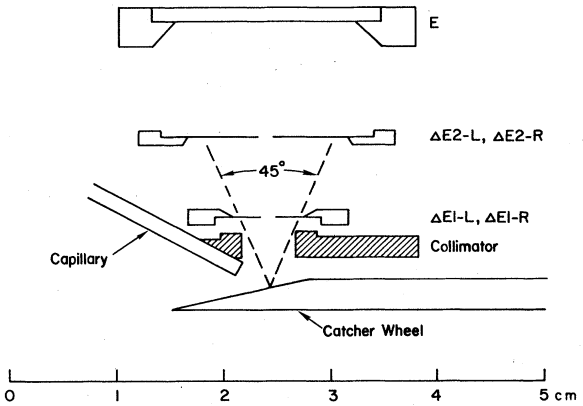

FIG. 4. Schematic diagram of the small angle detector system.

Figure 4 is a schematic diagram of the "small angle" detector system. This system was a three element semiconductor particle telescope (14—31 μm ΔE1, 155—170 μm ΔE2, 500—1000 μm E) with each circular ΔE detector fabricated such that the surface contact on one side was divided on the center line. This effectively produced two detectors on the same silicon wafer which will be re-

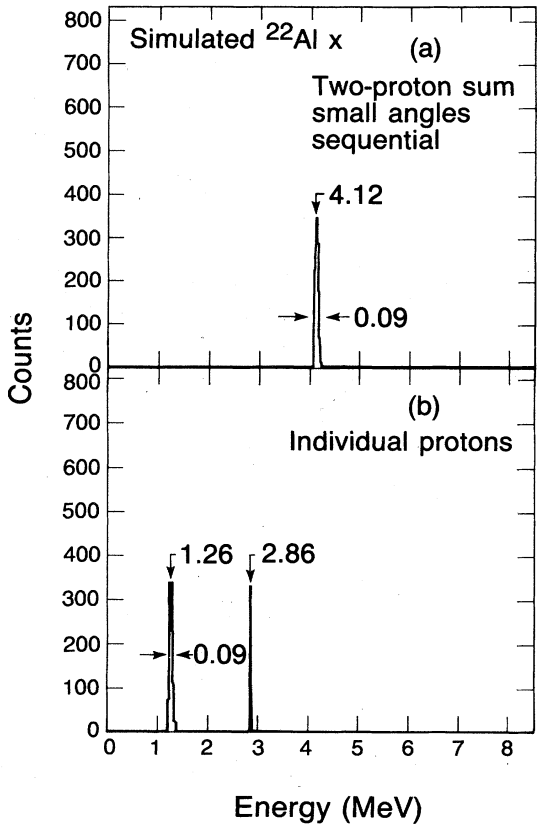

FIG. 5. Monte Carlo simulation of sequential emission of two protons as observed with the small angle detector system. See the text. (a) Two-proton summed energy spectrum. (b) Individual proton energy spectrum. Peak heights are arbitrarily normalized to lower energy group for display purposes.

ferred to as "left" (L) and "right" (R) detectors. Such an arrangement could detect low energy protons (typically $\sim$1.0–4.5 MeV) as $\Delta E1,\Delta E2$ coincidences in either the left or right sides or high energy protons (typically 4.7–9.0 MeV) as $\Delta E1,\Delta E2,E$ coincidences. Most importantly, particle-identified proton-proton coincidences could be observed between the left and right sides with a timing resolution typically better than 10 ns (FWHM).

Each two element, low energy telescope (e.g., $\Delta E1$-L and $\Delta E2$-L) subtended 4.5% of 4π sr, and each three element, high energy telescope subtended 1.5% of 4π sr (these high energy telescopes share the common, unsplit E detector). Since the left and right telescopes were separated by only a small distance, protons with a relative laboratory angle very close to $\eta=0°$ could be detected. The largest angle that could be detected was about $\eta=70°$, with the weighted average for the system being $\eta\sim45°$. This arrangement was chosen primarily because (a) it is desirable to subtend the largest possible solid angles in order to increase the sensitivity to these low yield activities as the effective delayed proton cross sections for ^{22}Al and ^{26}P are a few nanobarns and (b) a small angle system has the advantage of being able to detect the correlated protons from ^{2}He emission as well as the expected approximately isotropic distribution of a sequential emission.

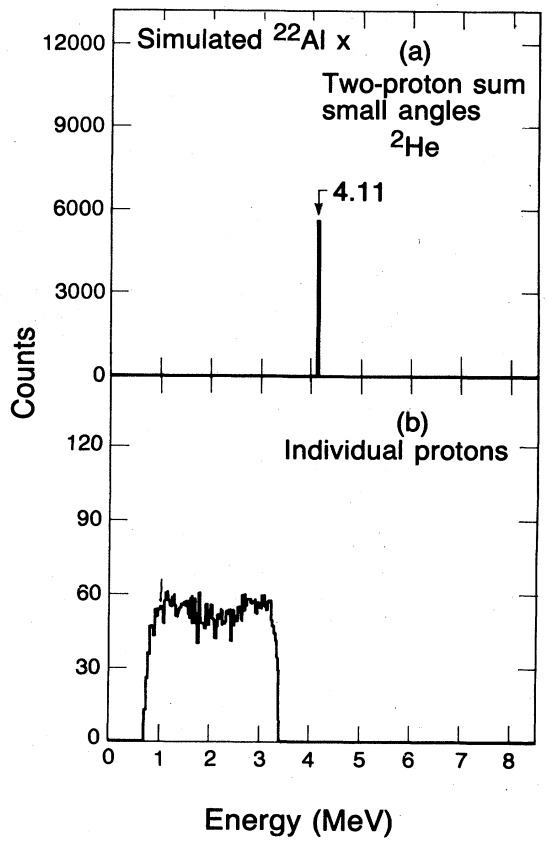

FIG. 6. Monte Carlo simulation of ^{2}He emission of two protons as observed with the small angle detector system. See the text. (a) Two-proton summed energy spectrum. (b) Individual proton energy spectrum.

Equations (1) and (2) show that for the decay energies involved for ^{2}He emission from ^{22}Al and ^{26}P, and assuming $\epsilon\sim500$ keV, the maximum (and most probable) value of η occurs at $\eta\sim40°$; therefore, this small angle system should be an excellent tool with which to search for either ^{2}He or sequential emission.

Monte Carlo simulations of expected observable proton-proton coincidence data for the small angle detector system are shown in Figs. 5 and 6. Figure 5 shows the expected two-proton sum spectrum and the spectrum of the individual protons contributing to the sum, for a sequential two-proton emission mechanism for ^{22}Al. The specific transition calculated is from the $T=2$ analog state in ^{22}Mg to the first excited state in ^{20}Ne (to be referred to as the ^{22}Al x transition) via a hypothetical intermediate state placed such that the first proton has a 3 MeV center-of-mass decay energy. Perfect detector energy resolution is assumed in order to show laboratory energy changes due solely to kinematic effects. It can be seen that the first proton (p_1) is emitted with a well-defined, easily calculable laboratory energy as in single proton emission or alpha decay. The second proton (p_2), however, has a laboratory energy dependent upon the center-of-mass angle between p_1 and p_2 [see Eq. (3)] so that its observed energy appears as a distribution determined by the spread in observable laboratory angles and the relative detection efficiency as a function of angle. (The reader should keep in mind that these detectors subtend large solid angles.)

Figure 6 presents the same type of simulation assuming a ^{2}He emission mechanism. A fixed value of $\epsilon=500$ keV was chosen for this example and the assumption was made that the ^{2}He breakup occurs relatively far from the nucleus (see Sec. II). These simplifications do not qualitatively affect the spectra obtained. The two-proton sum spectrum is seen to be very similar to that obtained in the calculation for sequential emission (the difference in width of the peaks will not be a strong distinguishing feature due to the individual telescope resolution of $\sim$50 keV FWHM); however, the individual proton spectrum is quite different. For ^{2}He emission, a continuum of individual proton energies centered at $E_{p_1}=E_{p_2}$ is expected. This distribution is maximized for the most probable emission of $E_{p_1}=E_{p_2}$ if the detectors are very large. Finite detector size produces a dip at this energy such as that shown in Fig. 6(b).

A simulation of preequilibrium two-proton emission, for the $\Delta t=0$ limit described in Sec. II, produces small angle spectra very similar to those for ^{2}He emission. The two-proton sum spectrum is a single relatively sharp peak and the individual proton energies are a continuum symmetric about $E_{p_1}=E_{p_2}$; however, in this case, the individual proton spectrum is always maximized at $E_{p_1}=E_{p_2}$.

A comparison of experimental data to these Monte Carlo simulations for the small angle detector system is presented in the following and will be shown to be quite useful, but in itself will not provide a conclusive characterization of the two-proton decay mechanism. More two-proton measurements made with a large angle detector system provided additional information; this system

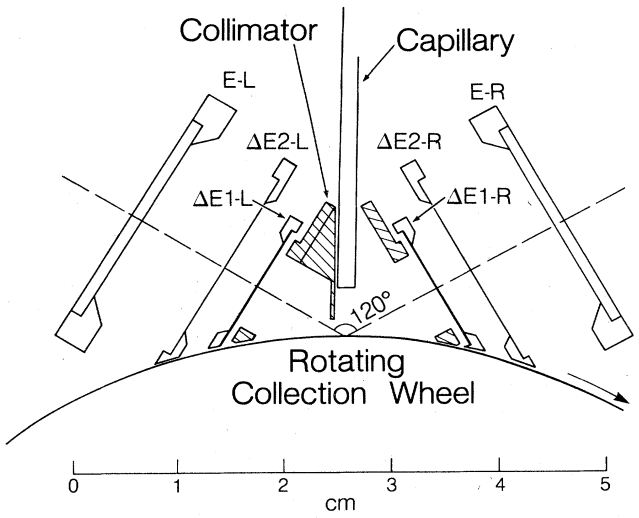

FIG. 7. Schematic diagram of the large angle detector system.

will be described next.

Figure 7 shows a schematic diagram of the large angle detector system. This arrangement consisted of two separate telescopes (ΔE_1 20—25 μm, $\Delta E2$ 200—250 μm, E 500—1000 μm). Both single protons and two-proton coincidences could be observed with this system in the same manner as that already described. The large angle detector system has an average angle $\eta = 120°$ between the circular telescopes and subtended 4.5% of 4π sr on each side for low energy protons (stopping in $\Delta E2$) and 3.0% of 4π sr on each side for high energy protons. This corresponds to a minimum detectable angle of $\eta = 70°$ and a maximum of $\eta = 170°$.

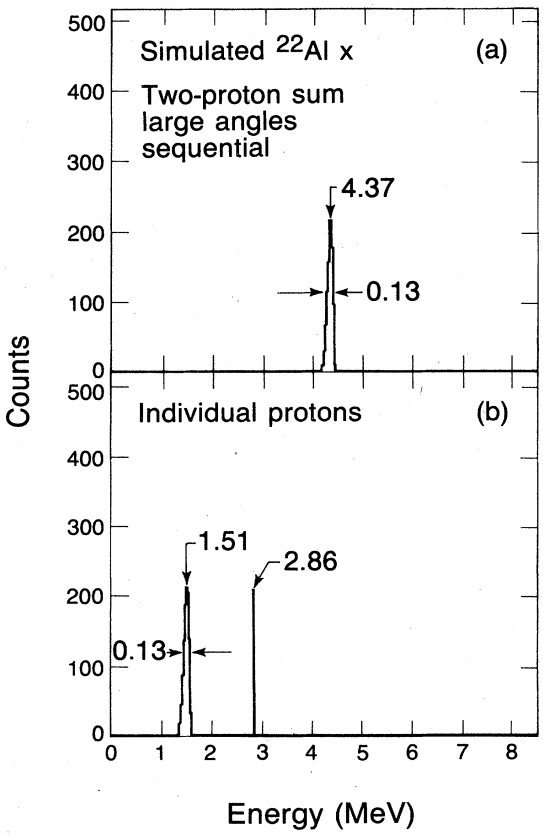

FIG. 8. Monte Carlo simulation of sequential emission of two protons as observed with the large angle detector system. See the text. (a) Two-proton summed energy spectrum. (b) Individual proton energy spectrum. Peak heights are arbitrarily normalized to lower energy group for display purposes.

A Monte Carlo simulation for a sequential two-proton emission (as already described) observed with the large angle detector system is shown in Fig. 8. Relative to the small angle data simulated in Fig. 5, it can be seen that for sequential emission a kinematic shift in the laboratory energy of the second proton is expected. This, of course, also causes a shift in the two-proton sum peak. There is also a broadening of the second proton peak due to the larger angular range covered by this system and the faster variation in the $\cos\theta$ term in Eq. (3) for this region.

^{2}He emission is not expected to be observable with the large angle detector system. Only much larger values of ϵ than those expected from Ref. 7 or 8 will produce a sufficiently large breakup angle for detection; therefore, any two-proton decays observed with this large angle detector system are expected to arise from a mechanism other than ^{2}He emission.

Simulation of $\Delta t = 0$ preequilibrium two-proton emission, which is not constrained to small angles, produces a two-proton sum peak at virtually the same energy as the shifted sum peak for sequential emission; however, the individual proton spectrum appears the same as at small angles.

To summarize all the mechanisms discussed, nearly identical two-proton sum peaks are expected in small and large angle experiments, with a measurable kinematic shift to higher energies at large angles (except for ^{2}He emission, which will not be observed at large angles). Individual proton spectra vary such that: (a) sequential emission will have discrete energy first and second proton groups, with the latter exhibiting the small to large angle kinematic shift; (b) ^{2}He emission will produce a continuum at small angles and will not be observable at large angles; and (c) $\Delta t = 0$ preequilibrium emission will produce a continuum at both large and small angles.

IV. RESULTS

Small and large angle measurements were made while bombarding Mg and Si targets in order to produce ^{22}Al and ^{26}P, respectively. Results of these measurements are displayed in Figs. 9—13, many of which represent the summation of several experiments. Summaries of the observed two-proton sum and individual proton energies are presented in Tables I and II.

For ^{22}Al, two two-proton groups were observed and are shown in Fig. 9(a). The observed two-proton sum energies are presented in Table I. Conversion of these laboratory energies to center-of-mass decay energies is dependent upon the two-proton emission mechanism and also upon details of the detector system, but these two groups can be shown to correspond to two-proton transitions from the $T = 2$ analog state in ^{22}Mg to the first excited and ground

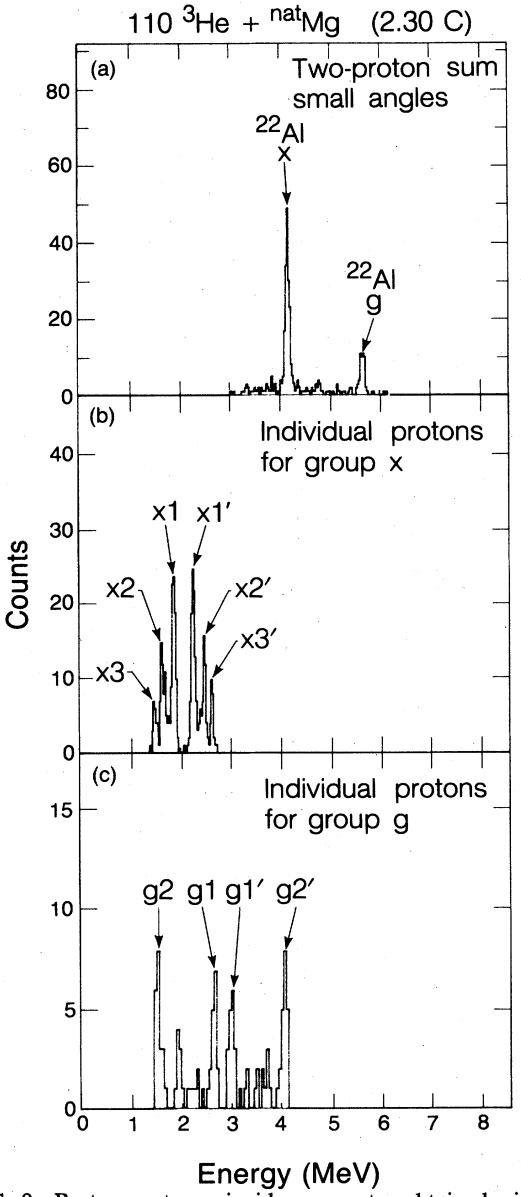

FIG. 9. Proton-proton coincidence spectra obtained with the small angle detector system following the decay of ^{22}Al. See the text. (a) Two-proton summed energy spectrum. Groups x and g correspond to transitions involving the ^{20}Ne first excited state and ground state, respectively. See Fig. 1. (b) Individual proton energy spectrum for protons forming group x in (a). (c) Individual proton energy spectrum for protons forming group g in (a).

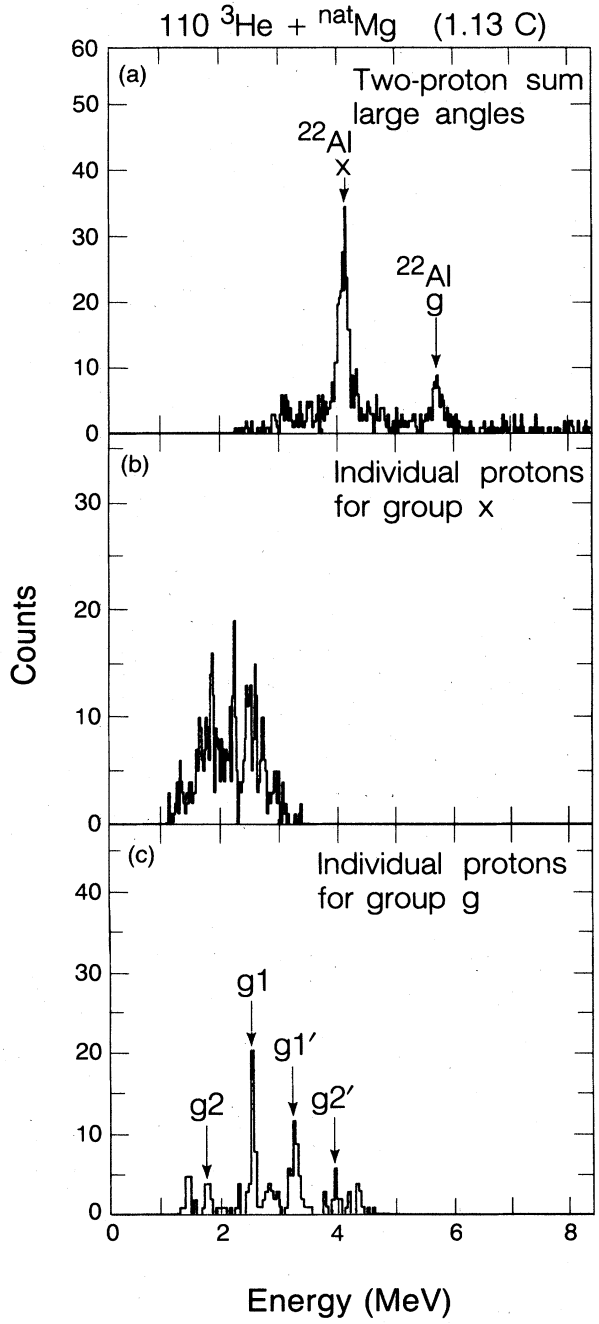

FIG. 10. Proton-proton coincidence spectra obtained with the large angle detector system following the decay of ^{22}Al. See the text. (a) Two-proton summed energy spectrum. Groups x and g correspond to transitions involving the ^{20}Ne first excited state and ground state, respectively. See Fig. 1. (b) Individual proton energy spectrum for protons forming group x in (a). (c) Individual proton energy spectrum for protons forming group g in (a).

states of ^{20}Ne (labeled x and g, respectively). Figures 9(b) and (c) are spectra of the individual protons making up these groups. They are obtained by gating on the indicated two-proton group, producing its "left" and "right" spectra (which are identical within statistics except for minor detector differences) and adding them together. It can be seen that both the x and g individual proton spectra appear to be composed of several discrete groups—the signature of a sequential decay mechanism. For the x group, three intermediate states in the proton daughter are involved, producing three pairs of proton groups (p_1 and p_2) labeled $x1$, $x1'$, etc. Only two intermediate states are readily identified for the g transition. These individual proton group energies are summarized in Table II.

Further evidence of the sequential nature of this decay

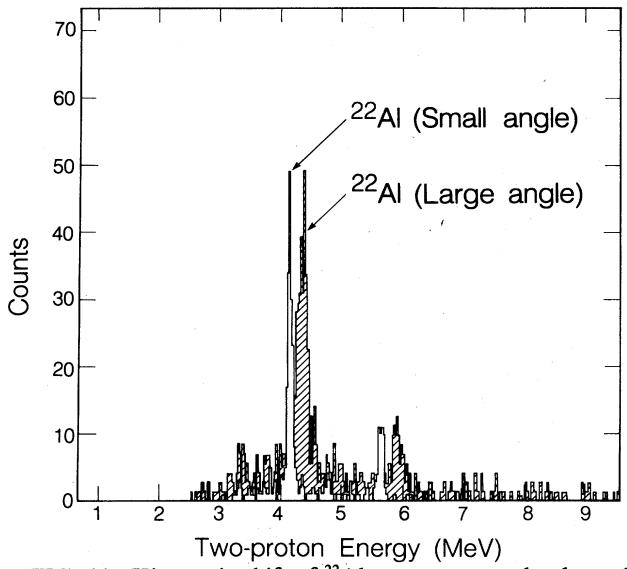

FIG. 11. Kinematic shift of ^{22}Al two-proton peaks shown by overlaying Figs. 9(a) and 10(a). Peak heights have been normalized to the small-angle measurement.

is seen by a comparison of the small and large angle measurements. Figure 10(a) shows the two-proton sum spectrum obtained for ^{22}Al with the large angle detector system; the small and large angle measurements are overlaid in Fig. 11. This figure clearly shows the kinematic shift of each two-proton group to higher energies, with the magnitude of each shift agreeing very well with that expected from Monte Carlo simulations already described [and also with a simple estimate obtainable from Eq. (3) using 45° and 120°]. Since it is the second proton energy that is shifted, it is, in principle, possible to identify the order of the decay (p_1 vs p_2) by a comparison of the small and large angle individual proton spectra. This works very well for the transitions involved in the g group (see Table II) and readily allows identification of groups $g1$ and $g2'$ as the first protons. Again, the energy shifts of the second protons agree very well with that expected for a sequential mechanism. A large angle measurement of the individual protons corresponding to the ^{22}Al x transition, however, produces the poorly resolved spectrum shown in Fig. 10(b). This precludes positive identification of the ordering of the proton pairs involved in the x transition; however, tentative assignments of $x1'$, $x2'$, and $x3'$ as first proton groups can be made. As seen in Table III (and as is discussed in more detail in the following), these tentative assignments also constitute a more reasonable decay scheme based on previously observed states in ^{21}Na than one built upon the alternative orderings.

The appearance of the large angle measurement of the ^{22}Al x transition shown in Fig. 10(b) is not fully understood. In general, the large angle measurements have poorer energy resolution than that of the small angle measurements due to (a) the poorer intrinsic resolution of the larger surface area (higher capacitance) $\Delta E1$ detectors used and (b) the kinematic broadening effect exhibited in the Monte Carlo simulations. These effects can be quite important since good energy and particle determinations

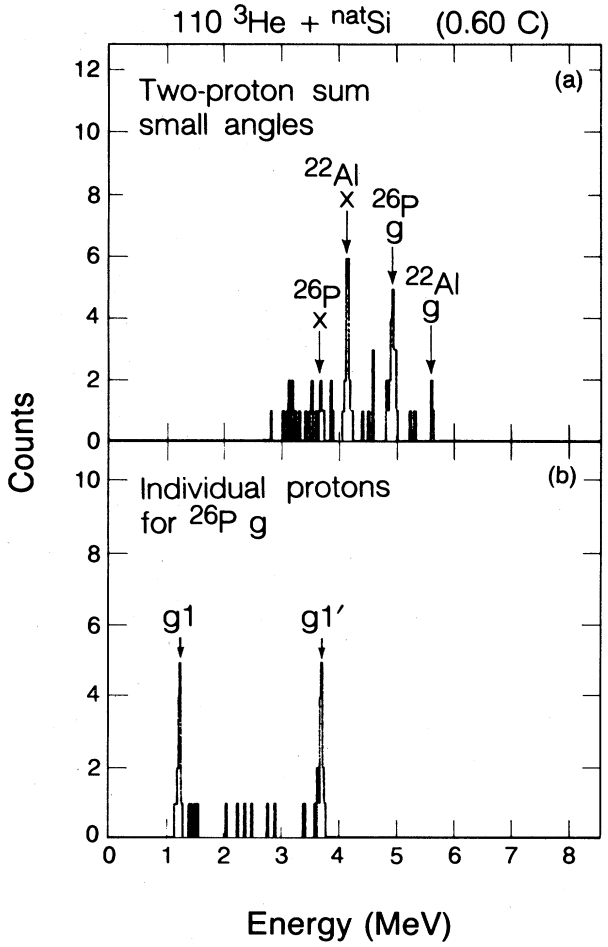

FIG. 12. Proton-proton coincidence spectra obtained with the small angle detector system following the decays of ^{22}Al and ^{26}P. See the text. (a) Two-proton summed energy spectrum containing both ^{22}Al and ^{26}P groups. (b) Individual proton energy spectrum for protons from the ^{26}P g group in (a). This group corresponds to a transition to the ^{24}Mg ground state (see Fig. 2).

are important for detection of these nanobarn cross section proton-proton coincidences in the high background present from beta and alpha particles, neutrons, gamma rays, etc.; however, this does not entirely explain this spectrum. There appears to be a possibility of a contribution from a continuum energy proton distribution, particularly since, as discussed in the following with respect to the 2p/1p ratio, there seem to be more two-proton events in this measurement than expected from the small angle work. Evidence for such a contribution is not strong, however, and would be difficult to explain, particularly since it is absent at small angles. A comparison of Figs. 9(c) and 10(c) also shows that the relative intensities of the ^{22}Al $g1$ and $g2$ proton pairs change. This may be at least partially due to differences in the variations of detector efficiencies with energy for the two detector systems, but may also indicate a stronger angular correlation than the 10—20% upper limit expected from standard calculations (these limits assume intermediate state spins up to $\frac{7}{2}$). Both of these features merit further investigation in future work.

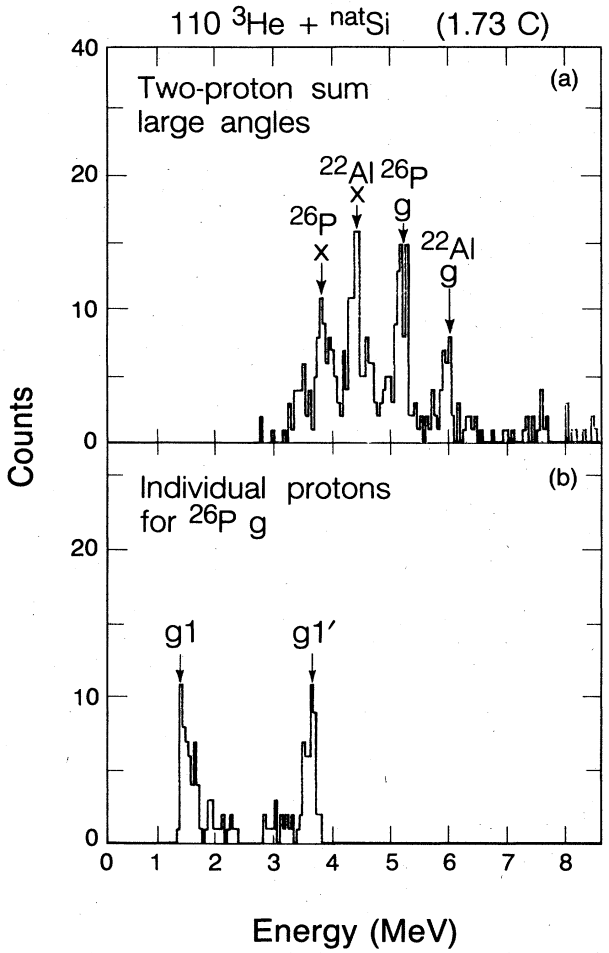

FIG. 13. Proton-proton coincidence spectra obtained with the large angle detector system following the decays of ^{22}Al and ^{26}P. See the text. (a) Two-proton summed energy spectrum containing both ^{22}Al and ^{26}P groups. (b) Individual proton energy spectrum for protons from the ^{26}P g group in (a). This group corresponds to a transition to the ^{24}Mg ground state (see Fig. 2).

Bombardments of Si produced not only the previously observed ^{22}Al x and g groups [from the ^{28}Si(^{3}He,αp4n)^{22}Al reaction] but, additionally, a new two-proton sum group corresponding to the two-proton transition from the $T=2$ analog state in ^{26}Si to the ground state of ^{24}Mg and labeled ^{26}P g in Figs. 12(a) and 13(a). The individual proton spectra corresponding to this group are shown in Figs. 12(b) and 13(b). This group again exhibits the signature of a sequential emission, this time through a single intermediate state in ^{25}Al. Tables I and II display the observed energies of these groups and show that $g1'$ is identifiable as the first proton. Kinematic shifts are again as expected from calculation. The expected location of the ^{26}P x two-proton sum peak is also labeled in Figs. 12(a) and 13(a). This group is too close to the low energy detection threshold, however, to measure reliably. It is only possible to say that some contribution is probably observed, particularly in the large angle measurement.

TABLE I. Observed two-proton sum energies.

Two-proton group	Small angle measurement	Large angle measurement
^{22}Al x	4.14(2)	4.35(3)
^{22}Al g	5.64(2)	5.93(3)
^{26}P g	4.92(2)	5.15(4)

With the individual proton energies in Table II, the sequence of emissions already described, and the mass excesses of the $T=2$ analog states (measured in Refs. 2 and 3), it is possible to determine the mass excesses of the intermediate states in the proton daughter nuclei. These results are displayed in Table III. For the ^{22}Al x transitions, where the ordering is uncertain, a mass excess is calculated for each possibility. Also included in Table III are the excitation energies of these intermediate states (calculated using proton daughter masses from Ref. 13) and a column headed "known states" which contains excitation energies of known proton daughter states (from Ref. 14) with energies close enough to those observed to possibly be the intermediate state. It can be seen that for each observed intermediate state, there is a corresponding, previously observed state (if the tentative ordering of the ^{22}Al x transitions, as already presented, is accepted). This does not, of course, conclusively identify these previously known states as the two-proton intermediate states, but it is likely that this is the case for most of the transitions. Decay schemes based on the information presented in Table III are shown in Figs. 14 and 15.

Two-proton branching relative to that of single proton emission (the 2p/1p ratio) can be determined, since, in addition to the two-proton coincidences, the detector systems used (see Sec. III) were also capable of detecting the higher energy (7–8 MeV) single proton groups of ^{22}Al and ^{26}P. These ratios are presented in Table IV. The single proton groups were observed with higher backgrounds than the measurements described in Refs. 2 and 3, howev-

TABLE II. Observed individual proton energies.

^{22}Al x		$x1$	$x1'$	$x2$	$x2'$	$x3$	$x3'$
	Small	1.88(2)	2.26(2)	1.66(2)	2.48(2)	1.48(2)	2.64(2)
^{22}Al g		$g1$	$g1'$	$g2$	$g2'$		
	Small	2.62(3)	2.98(3)	1.50(3)	4.05(3)		
	Large	2.61(3)	3.34(3)	1.82(3)	4.06(3)		
^{26}P g		$g1$	$g1'$				
	Small	1.21(2)	3.69(2)				
	Large	1.52(3)	3.64(3)				

TABLE III. Calculated proton-daughter state mass excesses and excitations.

Precursor	Assumed p_1 group	Mass[b] excess	E_x	Known[c] states	
^{22}Al	$\left[\frac{x1'}{x1}\right]$[a]	3.99(2) 4.39(2)	6.18(2) 6.58(2)	6.170(30)	$(\frac{1}{2}\text{-}\frac{7}{2})^+$
^{22}Al	$\left[\frac{x2'}{x2}\right]$[a]	3.76(2) 4.62(2)	5.95(2) 6.81(2)	5.979(15)	$(\frac{1}{2}\text{-}\frac{7}{2})^+$
^{22}Al	$\left[\frac{x3'}{x3}\right]$[a]	3.59(2) 4.81(2)	5.78(2) 7.00(2)	5.770(20) 7.060(30)	$(\frac{1}{2}\text{-}\frac{7}{2})^+$
^{22}Al	$g1$	3.62(3)	5.81(3)	5.770(20) 5.815	$(\frac{1}{2}\text{-}\frac{7}{2})^+$ $\frac{7}{2}^-$
^{22}Al	$g2'$	2.11(3)	4.30(3)	4.294(3)	$\frac{5}{2}^+$
^{26}P	$g1$	−5.20(2)	3.72(2)	3.6957(5)	$(\frac{7}{2}^-)$

[a]Ordering is uncertain. Underlined group is the more probable candidate.
[b]Calculated using small angle values.
[c]Known states from Ref. 14 that are close enough in energy to be possible intermediate states.

er, since some concessions in telescope design were necessary to allow detection of low energy two-proton coincidences (primarily, thinner $\Delta E1$ detectors were used than were optimum for high energy proton detection). This is probably the largest source of error in this 2p/1p ratio, followed by uncertainties in two-proton to single proton detection efficiencies and low counting statistics. Due to low counting statistics, all two-proton coincidences for each isotope's decay were summed rather than attempt a treatment of individual transitions. These ratios were calculated relative to the most intense single proton group known in each decay (7.839 MeV for ^{22}Al and 7.269 MeV for ^{26}P, laboratory energies) with an isotropic sequential emission of the protons assumed.

Absolute errors on these ratios are difficult to determine, but the 2p/1p values shown are thought to be reliable to within 50%. For ^{26}P, the 2p/1p ratio is close to unity and does not vary significantly from small to large angles. ^{22}Al has a higher 2p/1p ratio; however, the ^{22}Al

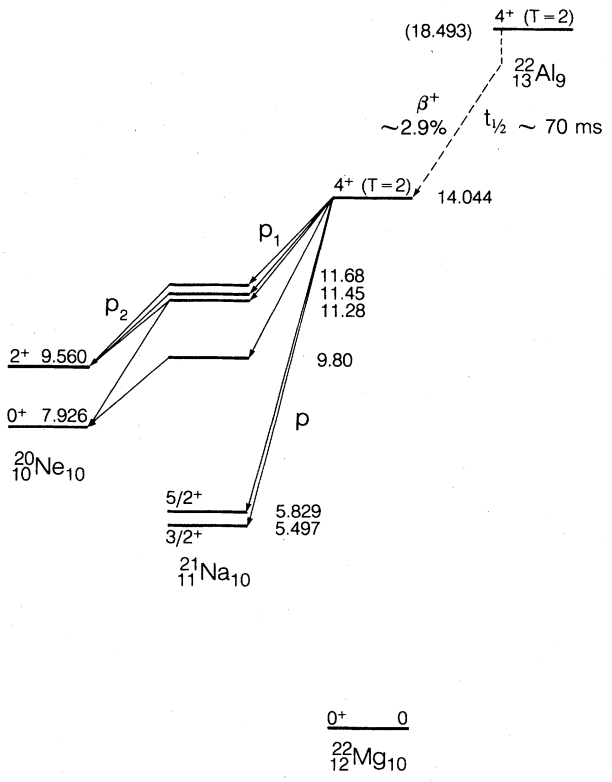

FIG. 14. Proposed new partial decay scheme for ^{22}Al.

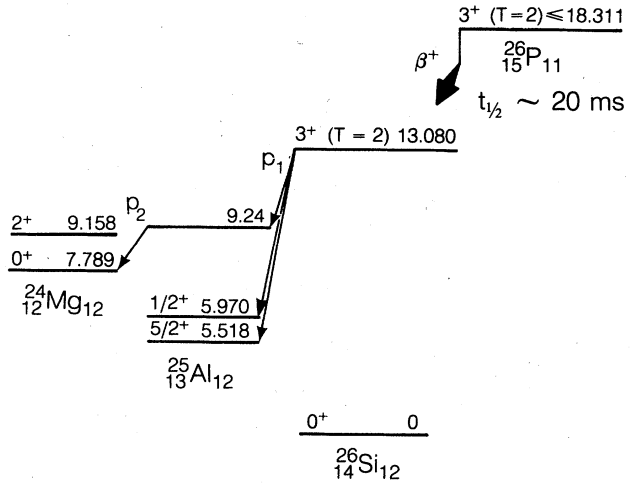

FIG. 15. Proposed new partial decay scheme for ^{26}P.

TABLE IV. $2_p/1_p$ ratios.

Isotope	Small angles	Large angles
^{22}Al	1.9	5.5
^{26}P	0.9	1.4

large angle measurement is significantly larger than the small angle measurement. This, in itself, might be ascribed to uncertainties in the measurement technique, but, as already discussed, the large angle ^{22}Al measurement has some other inconsistencies when compared to the observed spectrum at small angles. The most striking of these is the possibility of a continuum type of contribution to the ^{22}Al x individual proton spectrum shown in Fig. 9(b). The appearance of such a contribution at large angles would be very difficult to explain, given its absence at small angles [see Fig. 8(b)], but its presence could cause the variation in the 2p/1p ratio shown in Table IV. It is possible that this observation is due to an unidentified detector effect associated with the general difficulties of these nanobarn level experiments, but the possibility that this is due to some more interesting physical phenomenon should not be excluded.

V. SUMMARY

Beta-delayed two-proton radioactivity has been observed for the two nuclei ^{22}Al and ^{26}P. Two-proton coincidence experiments have been performed at small and large angles and have shown that the dominant two-proton emission mechanism is a sequential process. Possible decay schemes have been determined for each isotope. Some puzzling features of the large angle two-proton measurements for ^{22}Al decay have been observed and suggest further investigation.

Future work on beta-delayed two-proton radioactivity in general will be directed towards discovering new isotopes exhibiting this decay mode; the higher $T_z = -2$ nuclei ^{46}Mn and ^{50}Co are prime candidates. These studies may show that beta-delayed two-proton emission is not only an interesting phenomenon in itself, but may serve as a useful tool for detection and decay studies of new isotopes not observable by other techniques.

ACKNOWLEDGMENTS

We would like to thank J. Randrup for useful discussions of two-proton emission mechanisms and C. Maples, B. Rathbun, and D. Weaver for their help with the MIDAS computer system which was used in the data reduction. This work was supported by the U.S. Department of Energy under Contract No. DE-AC03-76SF00098.

*Present address: Department of Physics, University of Jyvaskyla, Jyvaskyla, Finland.

†Present address: Department of Physics, Nanjing University, Nanjing, China.

[1]V. I. Gol'danskii, Pis'ma Zh. Eksp. Teor. Fiz. **32**, 572 (1980) [JETP Lett. **32**, 554 (1980)].

[2]M. D. Cable, J. Honkanen, R. F. Parry, H. M. Thierens, J. M. Wouters, Z. Y. Zhou, and J. Cerny, Phys. Rev. C **26**, 1778 (1982).

[3]M. D. Cable, J. Honkanen, R. F. Parry, S. H. Zhou, Z. Y. Zhou, and J. Cerny, Phys. Lett. **123B**, 25 (1983).

[4]M. D. Cable, J. Honkanen, R. F. Parry, S. H. Zhou, Z. Y. Zhou, and J. Cerny, Phys. Rev. Lett. **50**, 404 (1983).

[5]J. Honkanen, M. D. Cable, R. F. Parry, S. H. Zhou, Z. Y. Zhou, and J. Cerny, Phys. Lett. **133B**, 146 (1983).

[6]V. I. Gol'danskii, Usp. Fiz. Nauk **87**, 255 (1965) [Sov. Phys. Usp. **8**, 770 (1966)].

[7]T. V. Congedo, I. S. Lee-Fan, and B. L. Cohen, Phys. Rev. C **22**, 985 (1980).

[8]D. P. Stahel, Ph.D. thesis, Lawrence Berkeley Laboratory Report No. LBL-9706, 1979.

[9]K. R. Symon, *Mechanics* (Addison-Wesley, Reading, Mass., 1971), p. 175.

[10]G. G. Ohlsen, Nucl. Instrum. Methods **37**, 240 (1965).

[11]L. C. Biedenharn, in *Nuclear Spectroscopy, Part B,* edited by F. Ajzenberg-Selove (Academic, New York, 1960), p. 732.

[12]C. Maples and J. Sivak, IEEE Trans. Nucl. Sci. **26**, 4409 (1979).

[13]A. H. Wapstra, G. Audi, and K. Bos, January 1982 Atomic Mass Table for Nuclides.

[14]P. M. Endt and C. van der Leun, Nucl. Phys. **A310**, 1 (1978).